Article

Cite This: *Biomacromolecules* XXXX, XXX, XXX−XXX

pubs.acs.org/Biomac

Apolipoprotein E Peptide-Guided Disulfide-Cross-Linked Micelles for Targeted Delivery of Sorafenib to Hepatocellular Carcinoma

Yingwen Li,[†,∥] Jingjing Wei,[†,∥] Yaohua Wei,[†] Liang Cheng,[*,†,‡] Beibei Guo,[†] Fenghua Meng,[*,†] Feng Li,[§] and Zhiyuan Zhong[*,†]

[†]Biomedical Polymers Laboratory, College of Chemistry, Chemical Engineering and Materials Science, and [‡]Department of Pharmaceutics, College of Pharmaceutical Sciences, Soochow University, Suzhou 215123, P. R. China

[§]Department of Respiratory Disease, Shanghai Public Health Clinical Center, Fudan University, Shanghai 201508, P. R. China

Supporting Information

ABSTRACT: Sorafenib (SF) is an FDA-approved molecular-targeted drug for treating hepatocellular carcinoma (HCC). SF, however, suffers from poor water solubility, low bioavailability, dose-limiting side effects, and possible drug resistance. Here, we report on apolipoprotein E peptide-decorated disulfide-cross-linked micellar SF (ApoE-Ms-SF) as a targeted and intelligent formulation for HCC therapy. ApoE-Ms-SF was prepared with a good SF loading of 7.0 wt %, small size (37 nm), high stability, and reduction-triggered drug release from poly(ethylene glycol)-*b*-poly(*ε*-caprolactone-*co*-dithiolane trimethylene carbonate)-mefenamate (PEG-P(CL-DTC)-MA) and ApoE-modified ApoE-PEG-P(CL-DTC) block copolymers. MTT assays in low-density lipoprotein receptors (LDLRs) overexpressing SMMC-7721 human liver cancer cells showed ApoE density-dependent antitumor potency of ApoE-Ms-SF, in which 7.5% ApoE led to the best antitumor effect (IC_{50}: 8.5 vs 23.3 μg/mL for free SF). Confocal studies, flow cytometry, western blot, and apoptotic assays illustrated clearly a more efficient uptake of ApoE-Ms than nontargeted Ms by SMMC-7721 cells as well as lower phosphorylated extracellular signal-regulated kinase protein level and better cell apoptosis caused by ApoE-Ms-SF compared with Ms-SF and free SF. ApoE-Ms-SF revealed a long circulation time (elimination half-life = 6.8 h). DiR-loaded ApoE-Ms showed a significantly higher accumulation in SMMC-7721 tumor than the nontargeted counterpart. The therapeutic outcomes in the orthotopic SMMC-7721 tumor models demonstrated that ApoE-Ms-SF reduced SF-associated side effects and brought about enhanced angiogenesis inhibition and tumor apoptosis compared to free SF and Ms-SF controls, leading to a better treatment of HCC.

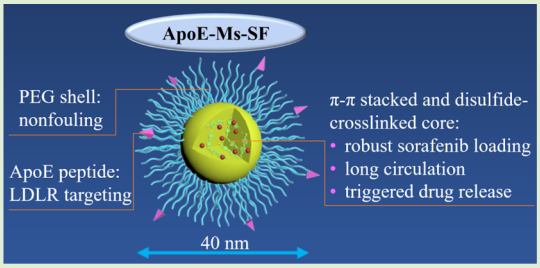

INTRODUCTION

Hepatocellular carcinoma (HCC) remains a clinical challenge though various treatments have been developed over the past decades.[1,2] Chemotherapy, with debatable benefits, becomes the treatment of choice for patients with advanced HCC that is metastatic or unable to be eradicated by surgery.[3] Nanomedicines have been conceived to enhance the anti-HCC efficacy of various chemical drugs like doxorubicin and paclitaxel.[4−6] The notorious toxicity of chemotherapeutics, though lessened by nanomedicines to a certain extent, could be detrimental to HCC patients, as their livers are extremely vulnerable.

Sorafenib (Nexavar, SF) is the first molecular-targeted drug approved by FDA for the treatment of unresectable or distally metastatic primary liver cancer.[7] SF, with a markedly lower toxicity than traditional chemotherapeutics, is able to delay HCC progression and prolong the patient survival from 7.9 to 10.7 months.[8] SF is a multitarget kinase inhibitor that can block RAF/MEK/extracellular signal-regulated kinase (ERK) cell signaling pathways, thereby inhibiting tumor cell growth, and inhibit vascular endothelial growth factor receptor and platelet-derived growth factor receptor pathways, thus inhibiting tumor angiogenesis.[9,10] SF, nevertheless, suffers from poor water solubility, low bioavailability, hematological and dermatological toxicities resulting from high oral doses applied in clinics (400 mg/day), and multidrug resistance.[11−13] In order to address the above issues, various nanocarriers including polymeric micelles, albumin, and lipid-based nanoparticles have been investigated for SF delivery.[14−21] Especially, actively targeted nanosystems that are functionalized with HCC-specific ligands such as lactobionic acid, galactose, folate, transferrin, GPC3 monoclonal antibody, and iRGD peptide have shown to improve the SF therapy for HCC models to varying degrees.[3,22−27] Unfortunately, most reported formulations reveal a low SF loading and poor stability that would demand an excessive amount of carrier materials and release SF prior to arrival at the target tumor site.

We herein report on ApoE peptide (LRKLRKRLLLRKLRKRLLC)-guided disulfide-cross-linked biodegradable polymeric micelles as a novel targeted vehicle

Received: October 14, 2019
Revised: November 21, 2019

DOI: 10.1021/acs.biomac.9b01419
Biomacromolecules XXXX, XXX, XXX−XXX

for SF (ApoE-Ms-SF) to achieve an enhanced HCC therapy (Scheme 1). ApoE-Ms-SF is self-assembled from poly(ethylene glycol)-*b*-poly(ε-caprolactone-*co*-dithiolane trimethylene carbonate)-mefenamate (PEG-P(CL-DTC)-MA) and ApoE-functionalized PEG-P(CL-DTC) (ApoE-PEG-P(CL-DTC)). MA is an anti-inflammatory analgesic agent. MA was introduced to enhance the loading of SF. We previously found that disulfide-cross-linked nanostructures based on DTC, while stable in circulation, quickly release drugs to the cytosols following uptake by cancer cells.[28−31] Apolipoprotein E and its derived ApoE peptide have high affinities to low-density lipoprotein receptors (LDLRs)[32] that are overexpressed in liver cancer cells[33,34] and glioma cells.[35,36] We assumed that ApoE-Ms-SF would mediate an enhanced delivery of SF to HCC.

Scheme 1. Illustration of ApoE Peptide-Guided Disulfide-Cross-Linked Biodegradable Micelles for Stable Loading and HCC-Targeted Delivery of SF

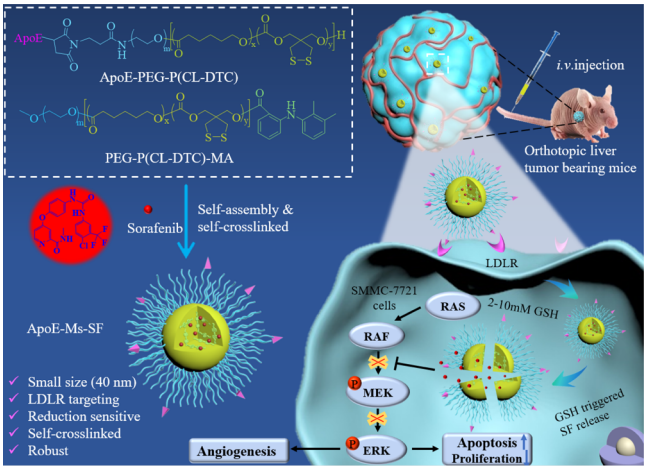

EXPERIMENTAL SECTION

Synthesis of PEG-P(CL-DTC)-MA and ApoE-PEG-P(CL-DTC). PEG-P(CL-DTC)-MA was synthesized by the esterification of PEG-P(CL-DTC), which was obtained with an M_n of 5.0 − (4.5 − 1.9) kg/mol as reported previously,[37] with MA. Briefly, dicyclohexyl carbodiimide (55 mg, 0.27 mmol) was added to MA (65 mg, 0.27 mmol) solution in dichloromethane (DCM, 2 mL) under stirring. After the reaction in the dark for 24 h at room temperature, the mixture was filtrated. The filtrate containing MA anhydride was added into 3 mL of DCM solution containing PEG-P(CL-DTC) (500 mg, 0.05 mmol)[37] and 4-dimethylaminopyridine (DMAP, 33 mg, 0.27 mmol) under stirring. After 48 h, PEG-P(CL-DTC)-MA was isolated by precipitation in cold diethyl ether/ethanol (4/1, v/v) twice and dried in a vacuum. Yield: 96%. ^{1}H NMR (600 MHz, DMSO-d_6): CL: δ 1.31, 1.53, 2.27, 3.98−4.05; DTC: δ 3.05, 4.05−4.13; PEG: δ 3.23, 3.51; MA: δ 2.09, 6.65−9.15. MA functionality was calculated to be 96% by ^{1}H nuclear magnetic resonance (NMR). The MA functionality of PEG-P(CL-DTC)-MA was also determined by ultraviolet absorption at 288 nm. The results revealed a functionality close to 100% based on a standard curve of known concentrations of MA.

ApoE-PEG-P(CL-DTC) was produced by coupling ApoE-SH peptide (LRKLRKRLLLRKLRKRLLC) to Mal-PEG-P(CL-DTC) via the Michael addition. First, using Mal-PEG-OH (M_n = 7.5 kg/mol) as an initiator and diphenyl phosphate (DPP) as a catalyst, Mal-PEG-P(CL-DTC) was obtained. Briefly, under a nitrogen atmosphere, Mal-PEG-OH (450 mg, 0.06 mmol), DTC (120 mg, 0.62 mmol), ε-CL (240 mg, 2.10 mmol), and DPP (150 mg, 0.60 mmol) were dissolved in 3 mL of anhydrous DCM and stirred for 48 h at 40 °C. Yield: 86%. ^{1}H NMR (600 MHz, DMSO-d_6): Mal: δ 7.0. M_n (^{1}H NMR) = 12.8 kg/mol, M_n (GPC) = 18.7 kg/mol, molecular weight distribution ($Đ$, GPC) = 1.1. Then, under a nitrogen atmosphere, ApoE-SH (73.4 mg, 0.03 mmol) was dropped to a stirring solution of Mal-PEG-P(DTC-CL) (200 mg, 0.02 mmol) in 4 mL of dimethyl sulfoxide (DMSO) at 37 °C. After 8 h, the mixture was dialyzed (MWCO 7000 Da) against DMSO for 24 h and DCM for 4 h before precipitation in cold diethyl ether. Yield: 82%. ^{1}H NMR (600 MHz, DMSO-d_6): ApoE: δ 0.8, 4.2−8.2. The functionality of ApoE was 98%, as determined by bicinchoninic acid (BCA) protein assay.

Preparation of ApoE-Ms and ApoE-Ms-SF. Ms-SF and ApoE-Ms-SF were prepared by the solvent displacement method. Briefly, a mixture of ApoE-PEG-P(CL-DTC) and PEG-P(CL-DTC)-MA (molar ratios ranging from 0/100, 5/95, 7.5/92.5 to 10/90) and a prescribed amount of SF in 200 μL of dimethylformamide (DMF) (10 mg/mL) was slowly added to 1 mL of phosphate buffer (PB, 10 mM, pH 7.4). After standing overnight at 37 °C, the mixture was dialyzed against PB (MWCO 7000 Da). The size, size distribution, and stability of ApoE-Ms-SF were measured using dynamic light scattering (DLS). The drug loading content (DLC) and drug loading efficiency (DLE) were determined with UV spectroscopy at 272 nm by adding ninefold DMF and incubating for 12 h before measurement. The empty ApoE-Ms or Ms was used as the background. The calibration curve was obtained from SF of known concentrations. DLC and DLE were calculated as below

$$\text{DLC (wt \%)} = \frac{\text{weight of loaded drug}}{\text{total weight of loaded drug and polymer}} \times 100$$

$$\text{DLE (\%)} = \frac{\text{weight of loaded drug}}{\text{weight of drug in feed}} \times 100$$

MTT Assays. Three human liver cancer cell lines, SMMC-7721 cells, HUH-7, and HepG2 cells, were seeded in 96-well plates (3×10^3 cells/well). After culturing under 5% CO_2 and 37 °C for 24 h, 20 μL of free SF (final SF concentration of 0.1−40 μg/mL) was added and incubated for 48 h. Then, MTT solution (10 μL, 5 mg/mL) was added and incubated for 4 h. After the removal of the medium, 150 μL of DMSO was added, and the absorbance of MTT formazan was determined by a microplate reader (Thermo Multiskan FC) at 570 nm. The cell viability was the percentage of the absorbance of the sample groups to that of the PBS group (n = 4).

To test the cytotoxicity of ApoE-Ms-SF and Ms-SF, SMMC-7721 cells and normal hepatocyte QSG-7701 were seeded in 96-well plates (3×10^3 cells/well). After 24 h, 20 μL of ApoE-Ms-SF, Ms-SF, or free SF in culture medium was added (final SF concentration: 0.1, 0.5, 1, 2, 4, 8, 10, 20, and 40 μg/mL). After 4 h, the medium was removed and the cells were further incubated in a fresh medium for 44 h. MTT assays were performed as described above. The toxicity of empty micelles (final polymer concentration: 10−200 μg/mL) to SMMC-7721 cells was tested similarly.

Cellular Uptake Studies of SMMC-7721 Cells. For flow cytometric measurements, the cells seeded in six-well plates (2×10^5 cells/well) overnight were incubated for 4 h with Cy5-labeled ApoE-Ms (ApoE-Ms-Cy5, 2 μg Cy5/mL) with different ApoE densities at 37 °C. The cells were digested by trypsin, centrifuged, washed with PBS (×2), and resuspended in 500 μL of PBS before immediate measurement using a flow cytometer for detecting Cy5 fluorescence.

For confocal laser scanning microscopy (CLSM) measurements, the cells seeded in 24-well plates (5×10^4 cells/well) overnight were incubated for 4 h with ApoE-Ms-Cy5 or Ms-Cy5 (40 μg Cy5/mL). The cells were fixed with 4% paraformaldehyde for 15 min and stained by 4′,6-diamidino-2-phenylindole with PBS washing (×3) after each step. The samples were observed using a confocal laser scanning microscope (TCS SP5).

Apoptosis Assays and Western Blot. SMMC-7721 cells seeded in six-well plates (3×10^5 cells/well) overnight were incubated for 4 h with ApoE-Ms-SF, Ms-SF, or free SF (6 μg SF/mL) and then with

DOI: 10.1021/acs.biomac.9b01419
Biomacromolecules XXXX, XXX, XXX−XXX

fresh medium for another 44 h. For apoptosis assays, the cells were washed and digested with ethylenediaminetetraacetic acid -free trypsin, centrifuged, washed (×3), and resuspended in 100 μL of binding buffer. A 5 μL of Annexin-V-Alexa Fluor 647 and 10 μL of PI solution were added successively. After 15 min, 400 μL of the binding buffer was added, followed by immediate flow cytometric measurements.

For western blot assays, the cells were washed, digested, centrifuged, and then lysed in a cell lysis buffer containing protease and phosphatase inhibitors at 4 °C for 20 min. The lysates were centrifuged (12 000 rpm, 15 min, 4 °C), and the supernatant concentration of proteins was quantified using a BCA protein analysis kit. The supernatants were adjusted to the same protein concentration by mixing with the buffer and boiled for 5 min. Soluble protein (40 μg) was separated by electrophoresis on a sodium dodecyl sulfate polyacrylamide gel electrophoresis gel and transferred onto polyvinylidene fluoride membranes (0.45 μm). At room temperature, 5% skimmed milk powder was used to seal up for 2 h. Then, antihuman rabbit phosphorylated ERK (pERK) (1:2000 dilution) was incubated with the cells overnight at 4 °C, and goat antirabbit IgG (1:20 000 dilution) was incubated for 1 h at 25 °C with the TBST (Tris-buffered saline, 0.1% Tween 20) solution (×3) washing after each step. Finally, the chemical signal was detected by a hypersensitive chemiluminescence gel imager (enhanced chemiluminescence).

Animal Models. All animals were handled under protocols approved by Soochow University Laboratory Animal Center and the Animal Care and Use Committee of Soochow University. Female Balb/c mice (5 weeks) were used for pharmacokinetics. For biodistribution studies, in vivo imaging, and antitumor therapy experiments, female nude mice (5 weeks) were used to build SMMC-7721 liver tumor models as previously reported.[29] Briefly, for establishing subcutaneous or orthotopic SMMC-7721 liver tumor models, 50 μL of SMMC-7721 cells (2×10^6/mouse) in PBS were mixed with 30% Matrigel and implanted into the right hind flank or the right upper liver lobe of the mice, respectively.

In Vivo Pharmacokinetic Studies. Healthy mice were divided into two groups ($n = 3$) and intravenously (iv) injected with 200 μL of ApoE-Ms-SF or Ms-SF (6 mg SF equiv/kg) via the tail veins. At fixed time points, 75 μL of blood was taken from the ophthalmic vein into a heparinized tube. A 20 μL of plasma was collected and added into DMF solution containing 20 mM dithiothreitol (DTT) to extract SF at 37 °C overnight. The SF concentrations in the solutions were detected by high-performance liquid chromatography (HPLC) with acetonitrile/0.1% trifluoroacetic acid aqueous solution (60/40, v/v) as an eluent.

Fluorescence Imaging and Biodistribution in Vivo. Female Bab/c mice bearing subcutaneous (tumor volume of 200−300 mm^3) or orthotopic (20 days after inoculation) SMMC-7721 tumors were grouped ($n = 3$) and iv injected with 200 μL of Ms-DiR or ApoE-Ms-DiR (4 μg DiR equiv/kg) via tail veins. At 2, 4, 8, 10, or 12 h post injection, the mice were scanned using a near-infrared fluorescence imaging system (ex. 747 nm, em. 774 nm) to acquire in vivo images.

For ex vivo imaging, at 10 h post injection, the orthotopic tumor models were sacrificed. The major organs and tumors were excised, washed, wiped, and weighed before imaging. In order to quantify the biodistribution of the drug, the tissues were homogenized and DiR was extracted by the DMF solution (containing 20 mM DTT) overnight. After centrifugation (12 000 rpm, 20 min), the DiR concentrations in the supernatants were determined by fluorometry ($n = 3$).

In Vivo Antitumor Efficacy. After 12 days of inoculation of the orthotopic tumor, the mice were arbitrarily allocated into five groups ($n = 5$). ApoE-Ms-SF (5 and 10 mg SF equiv/kg), Ms-SF (5 mg SF equiv/kg), free SF (5 mg SF equiv/kg), and PBS were iv injected every 3 days (total 8 injections). The mice were weighed every 2 days and normalized to the initial weights ($n = 5$). On day 27, one mouse of each group was sacrificed and major organs were collected and prepared for photographs and hematoxylin and eosin (H&E) staining. The tumors were carefully excised from the livers and sliced for H&E, terminal deoxynucleotidyl transferase dUTP nick end labeling (TUNEL), and CD34 staining using standard methods. The rest of the four mice were used for monitoring the survival rates.

Statistics. Data are presented as mean ± standard deviation (SD). One-way analysis of variance (ANOVA) with the Tukey multiple comparison test (Prism) was used to assess the difference among the groups. $*p < 0.05$ was considered significant, and $**p < 0.01$ and $***p < 0.001$ were highly significant.

RESULTS AND DISCUSSION

Synthesis of PEG-P(CL-DTC)-MA and ApoE-PEG-P(CL-DTC). PEG-P(CL-DTC)-MA was synthesized via ring-opening copolymerization of ε-CL and DTC as reported,[37] followed by esterification with MA (Figure S1, Table S1). MA was introduced to the end of PEG-P(CL-DTC) to enhance SF loading via π−π stacking in addition to hydrophobic interaction.[38,39] PEG-P(CL-DTC) was obtained with an M_n of 5.0 − (4.5 − 1.9) and a narrow molecular weight distribution ($Đ$) of 1.2, as reported previously.[37] The ^{1}H NMR spectrum of PEG-P(CL-DTC)-MA (Figure 1A) showed the characteristic peaks of PEG (δ 3.23 and 3.51), CL (δ 1.31, 1.53, 2.27, and 3.98−4.05), DTC (δ 3.05, 4.05−4.13), and MA moieties (δ 2.09, 6.65−9.15). The integral ratio of δ 2.09 (*o*-methyl protons of MA) and δ 3.51 (methylene protons of PEG) pointed out a high MA functionality of 96%. Ultraviolet measurements at 288 nm of PEG-P(CL-DTC)-MA confirmed a nearly quantitative functionality of MA (Figure S2).

The ApoE-PEG-P(CL-DTC) block copolymer was obtained via ring-opening polymerization (ROP) of DTC and CL initiated by Mal-PEG-OH (M_n = 7.5 kg/mol), yielding Mal-PEG-P(CL-DTC), followed by the Michael addition with the ApoE-SH peptide (LRKLRKRLLLRKLRKRLLC). Figure 1B shows intact Mal groups, as revealed by comparing the signals at δ 7.0 (vinyl protons of maleimide) with those at δ 3.51 (methylene protons of PEG) in the ^{1}H NMR spectrum. An M_n of 7.5-(3.5-1.8) kg/mol was calculated for Mal-PEG-P(CL-DTC) by comparing the signals at δ 2.27 (methylene protons of CL) and δ 3.05 (methylene protons neighboring the disulfide of DTC). Gel permeation chromatography (GPC) measurements revealed an M_n of 18.7 kg/mol and a narrow $Đ$ of 1.1 (Table S1, Figure S3). Notably, ^{1}H NMR of ApoE-PEG-P(CL-DTC) displayed that the peaks of ApoE appeared at δ 0.8 and 4.2−8.2, whereas Mal signals completely disappeared (Figure 1C), indicating the quantitative functionalization of ApoE. BCA assays using previously reported methods[40] corroborated a high ApoE peptide functionality of ca. 98% (Figure S4).

Fabrication of ApoE-Ms-SF. ApoE-Ms-SF was readily fabricated from the co-self-assembly of PEG-P(CL-DTC)-MA, ApoE-PEG-P(CL-DTC), and SF in aqueous solutions at the ApoE-PEG-P(CL-DTC) molar ratios of 0, 5, 7.5, or 10%. Interestingly, all ApoE-Ms-SFs with different ApoE densities exhibited a good SF loading with 70.4−86.9% efficiency and up to 7.0 wt % (Table 1). For example, at a theoretical DLC of 8.0 wt %, ApoE-Ms achieved a DLC of 6.5 wt % and DLE of 86.9%. In comparison, under the same conditions, micelles without MA functionalization exhibited a much lower DLC of 4.8 wt % and DLE of 63.0%, confirming that MA enhances SF loading likely via additional hydrophobic interaction and π−π stacking. The SF loading content had a little effect on the size and polydispersity index (PDI), in which ApoE-Ms-SF with 7.0 wt % of SF displayed a size of 37 nm (PDI 0.1). As seen from the DLS results (Figure 2A), ApoE density also had no influence on the size and PDI of ApoE-Ms-SF. ApoE-Ms-SF

DOI: 10.1021/acs.biomac.9b01419
Biomacromolecules XXXX, XXX, XXX−XXX

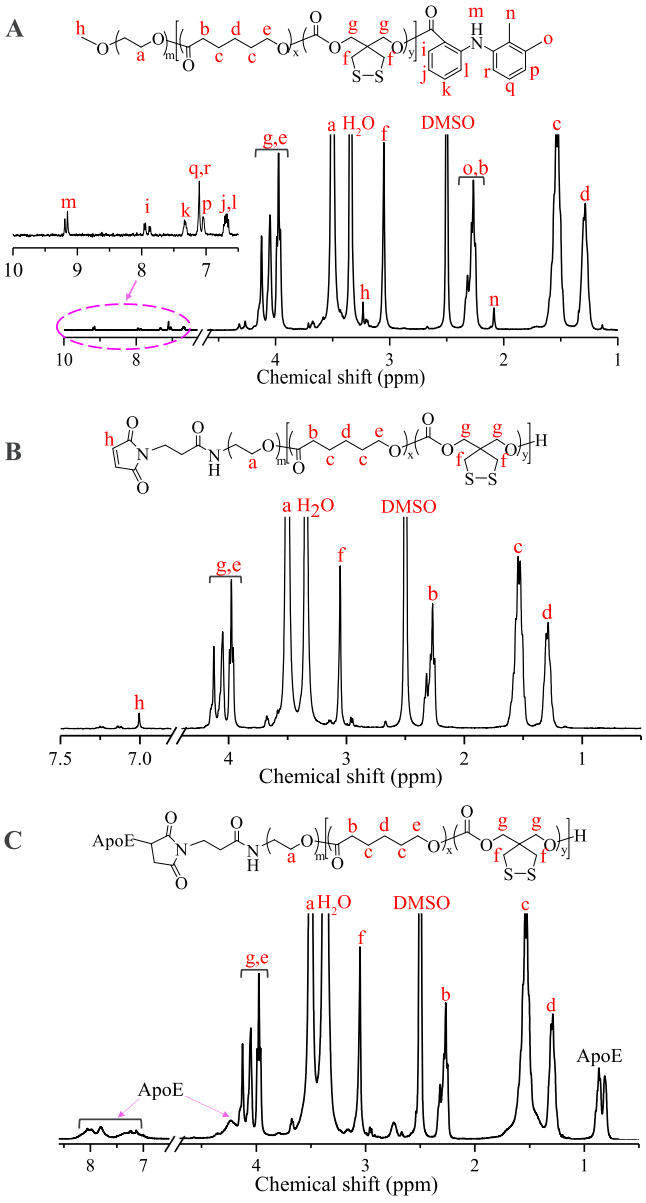

Figure 1. ^{1}H NMR spectra (600 MHz, DMSO-d_6) of PEG-P(CL-DTC)-MA (A), Mal-PEG-P(CL-DTC) (B), and ApoE-PEG-P(CL-DTC) (C).

Table 1. Characterization of Ms-SF and ApoE-Ms-SF

micelles	DLC (wt %) theory	DLC (wt %) determined[a]	DLE[a] (%)	size[b] (nm)	PDI[b]
Ms-SF	5	3.9	81.2	42	0.05
	8	6.0	79.7	42	0.05
	10	6.6	70.6	41	0.04
ApoE-Ms-SF[c]	5	3.4	70.4	41	0.03
	8	6.5	86.9	39	0.02
	10	7.0	75.2	37	0.10

[a]DLC and DLE were determined by a UV spectrometer. [b]The intensity−average size determined by DLS in PB (pH 7.4, 10 mM). [c]ApoE-Ms-SF with 7.5% ApoE.

was stable in 10% fetal bovine serum (FBS) (Figure S5B) and had no critical micellar concentration (Figure S5C), owing to the disulfide-cross-linking of micelles resulting from the spontaneous ROP of dithiolanes, as revealed by the significant

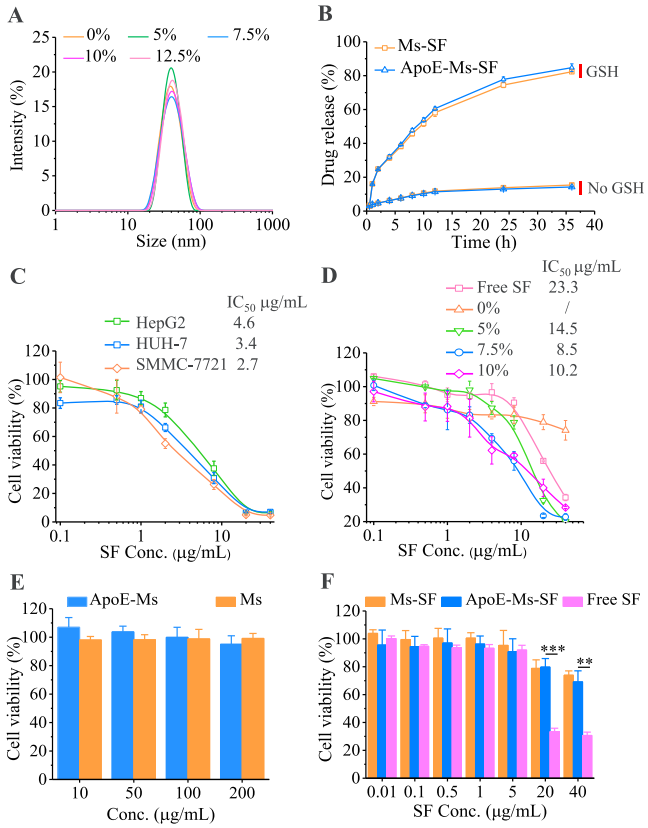

Figure 2. (A) Size and size distribution profiles of ApoE-Ms-SF with different ApoE surface densities in PB. (B) In vitro SF release from Ms-SF and ApoE-Ms-SF with or without 10 mM GSH. (C) Cytotoxicity of free SF on HepG2, HUH-7 and SMMC-7721 cells. (D) Viability of SMMC-7721 cells treated with Ms-SF and ApoE-Ms-SF with various ApoE ratios. (E) MTT assays of empty ApoE-Ms and Ms on SMMC-7721 cells. (F) Dependence of the viabilities of normal hepatocyte QSG-7701 cells on the concentrations of ApoE-Ms-SF, Ms-SF, or free SF. For (C,E), the incubation time was 48 h. For (D,F), the cells were incubated with drugs for 4 h and further cultured in a fresh medium for 44 h. For (B,D,F), ApoE-Ms-SF with 7.5% ApoE and 7.0 wt % SF was used.

decrease of characteristic UV absorption of dithiolane rings at 330 nm.[37,41] Upon adding 10 mM glutathione (GSH), ApoE-Ms-SF tended to swell (Figure S5D) because of the cleavage of the disulfide cross-links into free thiols.[42] Figure 2B shows that less than 15% SF was freed from ApoE-Ms-SF in 36 h under physiological conditions, whereas ca. 85% SF was released under 10 mM GSH, certifying the excellent stability and reduction-triggered SF release of ApoE-Ms-SF. This stable loading of SF under physiological conditions and triggered fast SF release in intracellular reductive conditions is advantageous over previously reported SF-loaded micelles.[43,44] The non-targeted micellar SF (Ms-SF) fabricated from PEG-P(CL-DTC)-MA exhibited practically the same biophysical and release properties of ApoE-Ms-SF (Table 1 and Figure 2B).

In Vitro Assessment of ApoE-Ms-SF and Ms-SF. We first evaluated the potency of free SF to three liver cancer cell lines, that is, HUH-7, HepG2, and SMMC-7721 cells, following 48 h of incubation. The results showed that free SF was potent to all the three cells, with IC_{50} ranging from 2.7 to 4.6 μg/mL (Figure 2C). SMMC-7721 cells were chosen to study the performance of ApoE-Ms-SF in vitro and in vivo. As revealed by MTT assays (Figure 2D), the antitumor potency of

DOI: 10.1021/acs.biomac.9b01419
Biomacromolecules XXXX, XXX, XXX−XXX

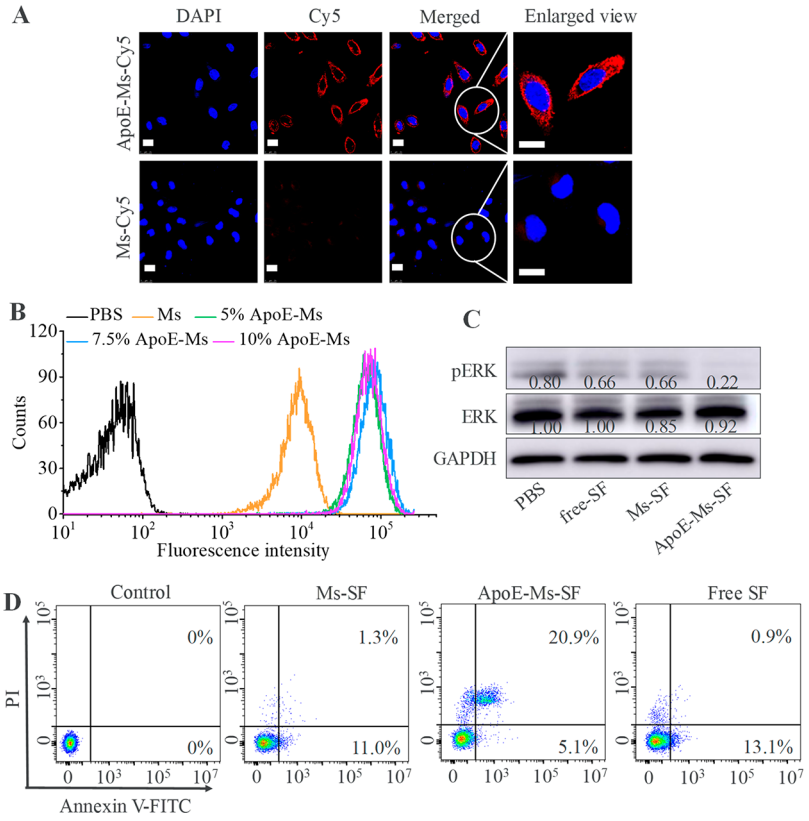

Figure 3. (A) CLSM images (40 μg Cy5/mL) and (B) flow cytometric analyses (2 μg Cy5/mL) of SMMC-7721 cells after 4 h incubation with ApoE-Ms-Cy5 of different ApoE contents. Scale bar: 25 μm. (C) Western blot analyses of pERK/ERK expression in SMMC-7721 cells treated with ApoE-Ms-SF, Ms-SF, free SF, or PBS. Glyceraldehyde 3-phosphate dehydrogenase was used as control. (D) Annexin V−FITC/PI staining assays of SMMC-7721 cells treated with ApoE-Ms-SF, Ms-SF, free SF, or PBS (SF: 6 μg/mL). For (C,D), the cells were incubated for 4 h and further cultured in a fresh medium for 44 h.

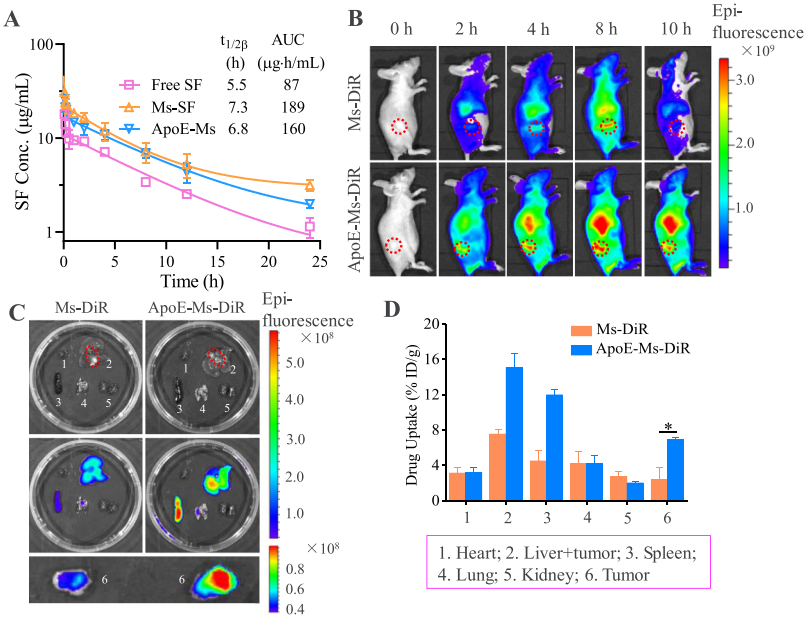

Figure 4. (A) Pharmacokinetics of free SF, Ms-SF, and ApoE-Ms-SF in Balb/c mice (SF: 6 mg/kg). (B) In vivo fluorescence images of subcutaneous SMMC-7721 tumor-bearing mice. Ex vivo fluorescence images (C) and quantitative distribution (D) of DiR in the major organs and tumors of orthotopic tumor-bearing mice at 10 h post injection. For (B−D), the mice were iv injected with 200 μL of ApoE-Ms-DiR or Ms-DiR (4 μg DiR/mouse).

ApoE-Ms-SF depended on the ApoE density, in which ApoE-Ms-SF with 7.5% ApoE displayed the highest antitumor activity (IC_{50} = 8.5 μg SF equiv/mL). Of note, here, SMMC-7721 cells after 4 h treatment with ApoE-Ms-SF were cultured

DOI: 10.1021/acs.biomac.9b01419
Biomacromolecules XXXX, XXX, XXX−XXX

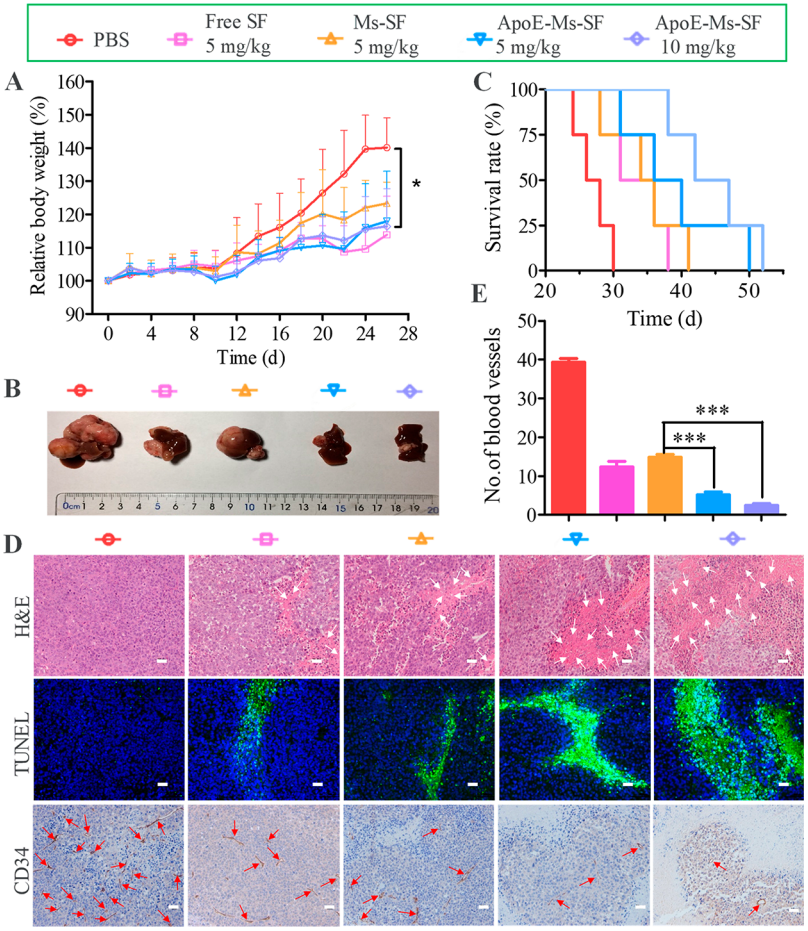

Figure 5. Antitumor efficacy of ApoE-Ms-SF in orthotopic SMMC-7721 tumor models. Mice were iv injected with ApoE-Ms-SF (5 or 10 mg/kg), Ms-SF (5 mg/kg), free SF (5 mg/kg), or PBS every 3 days (a total of eight injections). (A) Body weight changes (n = 5). (B) Photograph of the livers on day 27. (C) Survival curves (n = 4). (D) Microscopic images of H&E-stained, TUNEL-stained, and CD34-stained slices of tumors (20×). White and red arrowheads indicate the apoptotic cells and blood vessels, respectively. Scale bar: 20 μm. (E) Semiquantitative illustration of the number of blood vessels in six images. For A and E, *p < 0.05, ***p < 0.001 (one-way ANOVA and Tukey multiple comparison tests).

in fresh media for 44 h. Further increasing the ApoE density to 10% resulted in a lower antitumor activity, possibly because of the steric hindrance or receptor saturation effect. In comparison, the nontargeted Ms-SF had a cell viability of 74.1% even at a concentration of 40 μg SF equiv/mL. It is further noted that all ApoE-Ms-SF formulations were more potent than free SF (IC_{50} = 23.3 μg/mL). These results proved that ApoE has a clear targeting ability to SMMC-7721 cells. Apolipoprotein E has a high affinity to LDLR[32] that are overexpressed in liver cancer cells.[33] ApoE peptide screened from apolipoprotein E showed a targeting effect to LDLR.[34] ApoE-Ms-SF with 7.5% ApoE was selected for further studies. Both the empty ApoE-Ms and Ms were nontoxic at a concentration of 200 μg/mL (Figure 2E). Notably, in contrast to free SF that caused a significant death of normal liver cells at 20−40 μg/mL, both Ms-SF and ApoE-Ms-SF revealed a greatly reduced toxicity (Figure 2F). Hence, ApoE-Ms-SF has not only increased the antitumor efficacy but also spared healthy liver cells.

The internalization of Cy5-labeled ApoE-Ms (ApoE-Ms-Cy5) was studied in SMMC-7721 cells. The CLSM images displayed that ApoE-Ms-Cy5 was efficiently internalized and distributed in the cytosol within 4 h (Figure 3A). In contrast, little Cy5 fluorescence was detected for Ms-Cy5. The flow cytometric analyses revealed over a ninefold better uptake of ApoE-Ms-Cy5 than Ms-Cy5 (Figure 3B). Among the three ApoE-Ms-Cy5 with different ApoE densities, ApoE-Ms-Cy5 with 7.5% ApoE induced a slightly higher cell uptake, in line with the MTT results (Figure 2D).

Western blot experiments showed that the pERK expression in SMMC-7721 cells was markedly reduced by ApoE-Ms-SF, whereas the expression of ERK was barely changed (Figure 3C). It is known that pERK is a key component of the RAF/MEK/ERK signaling pathway, and SF can block this pathway and inhibit the phosphorylation of ERK, thereby inhibiting the proliferation of cancer cells.[45,46] The blockage of RAF/MEK/ERK cell signaling pathways would lead to apoptosis.[47] Flow cytometry analysis using Annexin V− fluorescein isothiocyanate (FITC)/*propidium iodide (PI)* staining displayed that ApoE-Ms-SF provoked a much higher cell apoptosis than Ms-SF and free SF (26.0% vs 12.3% and 14.0%) (Figure 3D). Moreover, mainly late apoptosis was discerned for ApoE-Ms-SF, whereas free SF and Ms-SF induced mostly early apoptosis, which was possibly because of the enhanced uptake of ApoE-Ms-SF and high intracellular SF concentration.

In Vivo Pharmacokinetics and Biodistribution. The concentration of SF in the blood of Balb/c mice measured using HPLC showed a two-compartment model with long elimination half-lives ($t_{1/2,\beta}$) of 7.3 and 6.8 h for Ms-SF and ApoE-Ms-SF, respectively (Figure 4A), supporting a high

DOI: 10.1021/acs.biomac.9b01419
Biomacromolecules XXXX, XXX, XXX−XXX

stability of ApoE-Ms-SF in vivo. Notably, an exceptional $t_{1/2,\beta}$ of ca. 5.5 h was also observed for free SF, likely because of the binding of SF to plasma proteins. The biodistribution was studied by applying an NIR dye DiR as a model. The in vivo imaging in subcutaneous SMMC-7721 tumor model displayed that ApoE-Ms-DiR started to accumulate in the tumor at 2 h post injection, peaked at 8 h, and reduced greatly at 10 h (Figure 4B). Ms-DiR only gathered very little in the tumor. In an orthotopic tumor model, the fluorescence intensity in the liver increased with time and the ApoE-Ms-DiR group was significantly higher than the Ms-DiR group at 4−12 h (Figure S6A). The ex vivo images at 12 h post injection displayed that the tumor fluorescence of the ApoE-Ms-DiR group was 2.9 times higher than that of the Ms-DiR group (Figure 4C). In order to quantify the drug biodistribution, the tumors and major organs were homogenized to extract DiR. The DiR content in the tumors of the ApoE-Ms-DiR group was ca. 6.9% ID/g, which was 2.8 times that of the Ms-DiR group (Figure 4D), confirming that ApoE has a good targeting ability to SMMC-7721 tumor. Of note, ApoE-Ms-DiR also showed an elevated DiR accumulation in the liver and spleen (Figures 4C and S6) because of their high expression of LDLR.[48] Although SF is a molecular-targeted drug, which might not cause severe side effects, its high accumulation in the liver and spleen remains a potential concern for ApoE peptide targeting.

Antitumor Activity of ApoE-Ms-SF in Orthotopic Liver Tumor Xenografts. The antitumor efficacy of ApoE-Ms-SF was evaluated at two SF doses (5 and 10 mg/kg) in orthotopic SMMC-7721 tumor models, with Ms-SF and free SF at 5 mg/kg as controls. The body weights and behavior of mice were monitored during treatment. The body weights of the PBS group increased quickly as from day 10, because of the development of ascites, illustrating the successful establishment of orthotopic liver tumor. ApoE-Ms-SF at either 5 or 10 mg/kg effectively suppressed ascites development, leading to a significantly less body weight increase (Figure 5A). The photos of liver excised on day 27 showed massive tumors in the liver of mouse treated with free SF and Ms-SF (Figure 5B). In contrast, only small tumors were found in the ApoE-Ms-SF-treated mice. In accordance, the ApoE-Ms-SF groups, especially at 10 mg/kg, exhibited better survival rates than free SF and Ms-SF groups (Figure 5C). H&E staining of the tumor slices detected more apoptosis for the ApoE-Ms-SF group than the Ms-SF and free SF groups (Figure 5D, upper row). Moreover, increasing the ApoE-Ms-SF dose from 5 to 10 mg/kg brought about a further increase of tumor cell death. TUNEL assays indicated that ApoE-Ms-SF induced a more massive apoptosis of tumor cells than Ms-SF and free SF (Figure 5D, middle row).

CD34 is a specific endothelial cell marker and has been commonly used for microvessel quantification in HCC.[49,50] The immunohistochemical analyses of tumor slices were done by staining with anti-CD34 antibody and *horseradish peroxidase*-labeled goat antirabbit secondary antibody. The images disclosed that ApoE-Ms-SF greatly reduced blood vessels in the tumor (Figure 5D, lower row). The semi-quantification of blood vessels in the tumor sections (Figure 5E) showed significantly less blood vessels in the ApoE-Ms-SF group compared with the free SF and Ms-SF groups. Hence, ApoE-Ms-SF not only enhances tumor cell death but also effectively inhibits neovascularization in the tumor. Of note, H&E histological analyses of major organs displayed that ApoE-Ms-SF did not cause significant damage to the spleen and liver (Figure S7), which is in line with the in vitro results that ApoE-Ms-SF has greatly reduced toxicity to normal liver cells (Figure 2F).

CONCLUSIONS

We have demonstrated that ApoE-decorated disulfide-cross-linked biodegradable micelles (ApoE-Ms) mediate enhanced SF therapy for orthotopic HCC in mice. SF-loaded ApoE-Ms (ApoE-Ms-SF) are unique in that they are small, robust, reduction-responsive, and specific to LDLR that are overexpressed in HCC cells. Interestingly, ApoE-Ms boosts the antitumor efficacy of SF to HCC cells but significantly reduces its toxic effect to healthy liver cells. ApoE-Ms-SF exhibits a long circulation time and effectively improved treatment of the orthotopic SMMC-7721 tumor model by inhibiting both pERK production and neovascularization in the tumors. ApoE-Ms-SF is potentially interesting for targeted SF therapy of HCC.

ASSOCIATED CONTENT

Supporting Information

The Supporting Information is available free of charge at https://pubs.acs.org/doi/10.1021/acs.biomac.9b01419.

Materials; methods; in vitro SF release; synthesis of PEG-P(CL-DTC)-MA and ApoE-PEG-P(CL-DTC); characterization of copolymers and ApoE-Ms; and in vivo imaging, biodistribution, and H&E analysis of major organs (PDF)

AUTHOR INFORMATION

Corresponding Authors

*E-mail: chengliang1983@suda.edu.cn. Phone/Fax: +86-512-65880098 (L.C.).
*E-mail: fhmeng@suda.edu.cn (F.M.).
*E-mail: zyzhong@suda.edu.cn (Z.Z.).

ORCID

Fenghua Meng: 0000-0002-8608-7738
Zhiyuan Zhong: 0000-0003-4175-4741

Author Contributions

‖Y.L. and J.W. contribute equally to this work.

Notes

The authors declare no competing financial interest.

ACKNOWLEDGMENTS

This work is supported by research grants from the National Natural Science Foundation of China (NSFC 51633005, 51761135117, 51861145310, 51561135010, 51773146).

REFERENCES

(1) Llovet, J. M.; Montal, R.; Sia, D.; Finn, R. S. Molecular therapies and precision medicine for hepatocellular carcinoma. *Nat. Rev. Clin. Oncol.* **2018**, *15*, 599−616.

(2) Ringelhan, M.; Pfister, D.; O'Connor, T.; Pikarsky, E.; Heikenwalder, M. The immunology of hepatocellular carcinoma. *Nat. Immunol.* **2018**, *19*, 222−232.

(3) Li, M.; Zhang, W.; Wang, B.; Gao, Y.; Song, Z.; Zheng, Q. C. Ligand-based targeted therapy: a novel strategy for hepatocellular carcinoma. *Int. J. Nanomed.* **2016**, *11*, 5645−5669.

(4) Sun, W.; Chen, X.; Xie, C.; Wang, Y.; Lin, L.; Zhu, K.; Shuai, X. T. Co-Delivery of Doxorubicin and Anti-BCL-2 siRNA by pH-Responsive Polymeric Vector to Overcome Drug Resistance in In

DOI: 10.1021/acs.biomac.9b01419
Biomacromolecules XXXX, XXX, XXX−XXX

Vitro and In Vivo HepG2 Hepatoma Model. *Biomacromolecules* **2018**, *19*, 2248−2256.
(5) Chen, W.; Zou, Y.; Meng, F. H.; Cheng, R.; Deng, C.; Feijen, J.; Zhong, Z. Y. Glyco-Nanoparticles with Sheddable Saccharide Shells: A Unique and Potent Platform for Hepatoma-Targeting Delivery of Anticancer Drugs. *Biomacromolecules* **2014**, *15*, 900−907.
(6) Yang, H. Y.; Jang, M.-S.; Gao, G. H.; Lee, J. H.; Lee, D. S. Construction of redox/pH dual stimuli-responsive PEGylated polymeric micelles for intracellular doxorubicin delivery in liver cancer. *Polym. Chem.* **2016**, *7*, 1813−1825.
(7) Bruix, J.; Raoul, J.-L.; Sherman, M.; Mazzaferro, V.; Bolondi, L.; Craxi, A.; Galle, P. R.; Santoro, A.; Beaugrand, M.; Sangiovanni, A. Efficacy and safety of sorafenib in patients with advanced hepatocellular carcinoma: subanalyses of a phase III trial. *J. Hepatol.* **2012**, *57*, 821−829.
(8) Bruix, J.; Cheng, A.-L.; Meinhardt, G.; Nakajima, K.; De Sanctis, Y.; Llovet, J. Prognostic factors and predictors of sorafenib benefit in patients with hepatocellular carcinoma: Analysis of two phase III studies. *J. Hepatol.* **2017**, *67*, 999−1008.
(9) Wilhelm, S.; Carter, C.; Lynch, M.; Lowinger, T.; Dumas, J.; Smith, R. A.; Schwartz, B.; Simantov, R.; Kelley, S. Discovery and development of sorafenib: a multikinase inhibitor for treating cancer. *Nat. Rev. Drug Discovery* **2006**, *5*, 835−844.
(10) Wilhelm, S. M.; Tang, L.; Wilkie, D.; McNabola, A.; Rong, H. BAY 43-9006 exhibits broad spectrum oral antitumor activity and targets the RAF/MEK/ERK pathway and receptor tyrosine kinases involved in tumor progression and angiogenesis. *Cancer Res.* **2004**, *64*, 7099−7109.
(11) Liu, C.; Chen, Z.; Chen, Y.; Lu, J.; Li, Y.; Wang, S.; Wu, G.; Qian, F. Improving Oral Bioavailability of Sorafenib by Optimizing the "Spring" and "Parachute" Based on Molecular Interaction Mechanisms. *Mol. Pharmaceutics* **2016**, *13*, 599−608.
(12) Cheng, A.-L.; Kang, Y.-K.; Chen, Z.; Tsao, C.-J.; Qin, S.; Kim, J. S.; Luo, R.; Feng, J.; Ye, S.; Yang, T.-S. Efficacy and safety of sorafenib in patients in the Asia-Pacific region with advanced hepatocellular carcinoma: a phase III randomised, double-blind, placebo-controlled trial. *Lancet Oncol.* **2009**, *10*, 25−34.
(13) Shen, Y.-C.; Ou, D.-L.; Hsu, C.; Lin, K.-L.; Chang, C.-Y.; Lin, C.-Y.; Liu, S.-H.; Cheng, A.-L. Activating oxidative phosphorylation by a pyruvate dehydrogenase kinase inhibitor overcomes sorafenib resistance of hepatocellular carcinoma. *Br. J. Cancer* **2013**, *108*, 72−81.
(14) Cao, H.; Wang, Y.; He, X.; Zhang, Z.; Yin, Q.; Chen, Y.; Yu, H.; Huang, Y.; Chen, L.; Xu, M.; Gu, W.; Li, Y. Codelivery of Sorafenib and Curcumin by Directed Self-Assembled Nanoparticles Enhances Therapeutic Effect on Hepatocellular Carcinoma. *Mol. Pharmaceutics* **2015**, *12*, 922−931.
(15) Thapa, R. K.; Choi, J. Y.; Poudel, B. K.; Hiep, T. T.; Pathak, S.; Gupta, B.; Choi, H. G.; Yong, C. S.; Kim, J. O. Multilayer-coated liquid crystalline nanoparticles for effective sorafenib delivery to hepatocellular carcinoma. *ACS Appl. Mater. Interfaces* **2015**, *7*, 20360−20368.
(16) Zhang, N.; Zhang, B.; Gong, X.; Wang, T.; Liu, Y.; Yang, S. In vivo biodistribution, biocompatibility, and efficacy of sorafenib-loaded lipid-based nanosuspensions evaluated experimentally in cancer. *Int. J. Nanomed.* **2016**, *11*, 2329−2343.
(17) Su, Y.; Wang, K.; Li, Y.; Song, W.; Xin, Y.; Zhao, W.; Tian, J.; Ren, L.; Lu, L. Sorafenib-loaded polymeric micelles as passive targeting therapeutic agents for hepatocellular carcinoma therapy. *Nanomedicine* **2018**, *13*, 1009−1023.
(18) Zhao, P.; Li, M.; Wang, Y.; Chen, Y.; He, C.; Zhang, X.; Yang, T.; Lu, Y.; You, J.; Lee, R. J.; Xiang, G. Enhancing anti-tumor efficiency in hepatocellular carcinoma through the autophagy inhibition by miR-375/sorafenib in lipid-coated calcium carbonate nanoparticles. *Acta Biomater.* **2018**, *72*, 248−255.
(19) Zheng, G.; Zhao, R.; Xu, A.; Shen, Z.; Chen, X.; Shao, J. Co-delivery of sorafenib and siVEGF based on mesoporous silica nanoparticles for ASGPR mediated targeted HCC therapy. *Eur. J. Pharm. Sci.* **2018**, *111*, 492−502.
(20) Zhang, J.; Wang, T.; Mu, S.; Olerile, L. D.; Yu, X.; Zhang, N. Biomacromolecule/lipid hybrid nanoparticles for controlled delivery of sorafenib in targeting hepatocellular carcinoma therapy. *Nanomedicine* **2017**, *12*, 911−925.
(21) Park, W.; Chen, J.; Cho, S.; Park, S. J.; Larson, A. C.; Na, K.; Kim, D. H. Acidic pH-Triggered Drug-Eluting Nanocomposites for Magnetic Resonance Imaging-Monitored Intra-arterial Drug Delivery to Hepatocellular Carcinoma. *ACS Appl. Mater. Interfaces* **2016**, *8*, 12711−12719.
(22) Zhao, R.; Li, T.; Zheng, G.; Jiang, K.; Fan, L.; Shao, J. Simultaneous inhibition of growth and metastasis of hepatocellular carcinoma by co-delivery of ursolic acid and sorafenib using lactobionic acid modified and pH-sensitive chitosan-conjugated mesoporous silica nanocomplex. *Biomaterials* **2017**, *143*, 1−16.
(23) Craparo, E. F.; Sardo, C.; Serio, R.; Zizzo, M. G.; Bondì, M. L.; Giammona, G.; Cavallaro, G. Galactosylated polymeric carriers for liver targeting of sorafenib. *Int. J. Pharm.* **2014**, *466*, 172−180.
(24) Li, Y.-J.; Dong, M.; Kong, F.-M.; Zhou, J.-P. Folate-decorated anticancer drug and magnetic nanoparticles encapsulated polymeric carrier for liver cancer therapeutics. *Int. J. Pharm.* **2015**, *489*, 83−90.
(25) Malarvizhi, G. L.; Retnakumari, A. P.; Nair, S.; Koyakutty, M. Transferrin targeted core-shell nanomedicine for combinatorial delivery of doxorubicin and sorafenib against hepatocellular carcinoma. *Nanomedicine* **2014**, *10*, 1649−1659.
(26) Tang, X.; Chen, L.; Li, A.; Cai, S.; Zhang, Y.; Liu, X.; Jiang, Z.; Liu, X.; Liang, Y.; Ma, D. Anti-GPC3 antibody-modified sorafenib-loaded nanoparticles significantly inhibited HepG2 hepatocellular carcinoma. *Drug Delivery* **2018**, *25*, 1484−1494.
(27) Zhang, J.; Hu, J.; Chan, H. F.; Skibba, M.; Liang, G.; Chen, M. iRGD decorated lipid-polymer hybrid nanoparticles for targeted co-delivery of doxorubicin and sorafenib to enhance anti-hepatocellular carcinoma efficacy. *Nanomedicine* **2016**, *12*, 1303−1311.
(28) Zhu, Y.; Jiang, Y.; Meng, F.; Deng, C.; Cheng, R.; Zhang, J.; Feijen, J.; Zhong, Z. Highly efficacious and specific anti-glioma chemotherapy by tandem nanomicelles co-functionalized with brain tumor-targeting and cell-penetrating peptides. *J. Controlled Release* **2018**, *278*, 1−8.
(29) Fang, Y.; Yang, W.; Cheng, L.; Meng, F.; Zhang, J.; Zhong, Z. EGFR-targeted multifunctional polymersomal doxorubicin induces selective and potent suppression of orthotopic human liver cancer in vivo. *Acta Biomater.* **2017**, *64*, 323−333.
(30) Zou, Y.; Zheng, M.; Yang, W.; Meng, F.; Miyata, K.; Kim, H. J.; Kataoka, K.; Zhong, Z. Virus-mimicking chimaeric polymersomes boost targeted cancer siRNA therapy in vivo. *Adv. Mater.* **2017**, *29*, 1703285.
(31) Zou, Y.; Fang, Y.; Meng, H.; Meng, F.; Deng, C.; Zhang, J.; Zhong, Z. Self-crosslinkable and intracellularly decrosslinkable biodegradable micellar nanoparticles: A robust, simple and multifunctional nanoplatform for high-efficiency targeted cancer chemotherapy. *J. Controlled Release* **2016**, *244*, 326−335.
(32) Chung, N. S.; Wasan, K. M. Potential role of the low-density lipoprotein receptor family as mediators of cellular drug uptake. *Adv. Drug Delivery Rev.* **2004**, *56*, 1315−1334.
(33) Kang, J.-H.; Toita, R.; Murata, M. Liver cell-targeted delivery of therapeutic molecules. *Crit. Rev. Biotechnol.* **2016**, *36*, 132−143.
(34) Wang, D.; El-Amouri, S. S.; Dai, M.; Kuan, C.-Y.; Hui, D. Y.; Brady, R. O.; Pan, D. Engineering a lysosomal enzyme with a derivative of receptor-binding domain of apoE enables delivery across the blood−brain barrier. *Proc. Natl. Acad. Sci. U.S.A.* **2013**, *110*, 2999−3004.
(35) Spencer, B. J.; Verma, I. M. Targeted delivery of proteins across the blood-brain barrier. *Proc. Natl. Acad. Sci. U.S.A.* **2007**, *104*, 7594−7599.
(36) Oller-Salvia, B.; Sánchez-Navarro, M.; Giralt, E.; Teixido, M. Blood−brain barrier shuttle peptides: an emerging paradigm for brain delivery. *Chem. Soc. Rev.* **2016**, *45*, 4690−4707.
(37) Fang, Y.; Jiang, Y.; Zou, Y.; Meng, F.; Zhang, J.; Deng, C.; Sun, H.; Zhong, Z. Targeted glioma chemotherapy by cyclic RGD peptide-functionalized reversibly core-crosslinked multifunctional poly-

DOI: 10.1021/acs.biomac.9b01419
Biomacromolecules XXXX, XXX, XXX−XXX

(ethylene glycol)- b -poly(ε-caprolactone) micelles. *Acta Biomater.* **2017**, *50*, 396−406.
(38) Shi, Y.; Van Der Meel, R.; Theek, B.; Oude Blenke, E.; Pieters, E. H.; Fens, M. H.; Ehling, J.; Schiffelers, R. M.; Storm, G.; Van Nostrum, C. F. Complete regression of xenograft tumors upon targeted delivery of paclitaxel via Π−Π stacking stabilized polymeric micelles. *ACS Nano* **2015**, *9*, 3740−3752.
(39) Gu, X.; Wei, Y.; Fan, Q.; Sun, H.; Cheng, R.; Zhong, Z.; Deng, C. cRGD-decorated biodegradable polytyrosine nanoparticles for robust encapsulation and targeted delivery of doxorubicin to colorectal cancer in vivo. *J. Controlled Release* **2019**, *301*, 110−118.
(40) Zhu, Y.; Zhang, J.; Meng, F.; Deng, C.; Cheng, R.; Feijen, J.; Zhong, Z. cRGD-functionalized reduction-sensitive shell-sheddable biodegradable micelles mediate enhanced doxorubicin delivery to human glioma xenografts in vivo. *J. Controlled Release* **2016**, *233*, 29−38.
(41) Zhang, X.; Waymouth, R. M. 1,2-dithiolane-derived dynamic, covalent materials: Cooperative self-assembly and reversible cross-linking. *J. Am. Chem. Soc.* **2017**, *139*, 3822−3833.
(42) Yang, W.; Zou, Y.; Meng, F.; Zhang, J.; Cheng, R.; Deng, C.; Zhong, Z. Efficient and targeted suppression of human lung tumor xenografts in mice with methotrexate sodium encapsulated in all-function-in-one chimeric polymersomes. *Adv. Mater.* **2016**, *28*, 8234−8239.
(43) Gao, D.-Y.; Lin, T.-T.; Sung, Y.-C.; Liu, Y. C.; Chiang, W.-H.; Chang, C.-C.; Liu, J.-Y.; Chen, Y. CXCR4-targeted lipid-coated PLGA nanoparticles deliver sorafenib and overcome acquired drug resistance in liver cancer. *Biomaterials* **2015**, *67*, 194−203.
(44) Chen, J.; Sheu, A. Y.; Li, W.; Zhang, Z.; Kim, D. H.; Lewandowski, R. J.; Omary, R. A.; Shea, L. D.; Larson, A. C. Poly(lactide-co-glycolide) microspheres for MRI-monitored trans-catheter delivery of sorafenib to liver tumors. *J. Controlled Release* **2014**, *184*, 10−17.
(45) Wang, C.; Jin, H.; Gao, D.; Lieftink, C.; Evers, B.; Jin, G.; Xue, Z.; Wang, L.; Beijersbergen, R. L.; Qin, W.; Bernards, R. Phospho-ERK is a biomarker of response to a synthetic lethal drug combination of sorafenib and MEK inhibition in liver cancer. *J. Hepatol.* **2018**, *69*, 1057−1065.
(46) Sung, Y.-C.; Liu, Y.-C.; Chao, P.-H.; Chang, C.-C.; Jin, P.-R.; Lin, T.-T.; Lin, J.-A.; Cheng, H.-T.; Wang, J.; Lai, C.-P.; Chen, L.-H.; Wu, A.-Y.; Ho, T.-L.; Chiang, T.; Gao, D.-Y.; Duda, D.-G.; Chen, Y. Combined delivery of sorafenib and a MEK inhibitor using CXCR4-targeted nanoparticles reduces hepatic fibrosis and prevents tumor development. *Theranostics* **2018**, *8*, 894−905.
(47) Liu, L.; Cao, Y.; Chen, C.; Zhang, X.; McNabola, A.; Wilkie, D.; Wilhelm, S.; Lynch, M.; Carter, C. Sorafenib Blocks the RAF/MEK/ERK Pathway, Inhibits Tumor Angiogenesis, and Induces Tumor Cell Apoptosis in Hepatocellular Carcinoma Model PLC/PRF/5. *Cancer Res.* **2006**, *66*, 11851−11858.
(48) Jeon, H.; Blacklow, S. C. Structure and physiologic function of the low-density lipoprotein receptor. *Annu. Rev. Biochem.* **2005**, *74*, 535−562.
(49) Poon, R. T.-P.; Ng, I. O.-L.; Lau, C.; Yu, W.-C.; Yang, Z.-F.; Fan, S.-T.; Wong, J. Tumor microvessel density as a predictor of recurrence after resection of hepatocellular carcinoma: a prospective study. *J. Clin. Oncol.* **2002**, *20*, 1775−1785.
(50) Frachon, S.; Gouysse, G.; Dumortier, J.; Couvelard, A.; Nejjari, M.; Mion, F.; Berger, F.; Paliard, P.; Boillot, O.; Scoazec, J.-Y. Endothelial cell marker expression in dysplastic lesions of the liver: an immunohistochemical study. *J. Hepatol.* **2001**, *34*, 850−857.

DOI: 10.1021/acs.biomac.9b01419
Biomacromolecules XXXX, XXX, XXX−XXX